Laser control of double proton transfer in porphycenes: towards an ultrafast switch for photonic molecular wires

Mahmoud K. Abdel-Latif · Oliver Kühn

Abstract Electronic excitation energy transfer along a molecular wire depends on the relative orientation of the electronic transition dipole moments of neighboring chromophores. In porphycenes, this orientation is changed upon double proton transfer in the electronic ground state. We explore the possibility to trigger such a double proton transfer reaction by means of an infrared pump-dump laser control scheme. To this end, a quantum chemical characterization of an asymmetrically substituted porphycene is performed using density functional theory. Ground state geometries, the topology of the potential energy surface for double proton transfer, and $S_0 \rightarrow S_1$ transition energies are compared with the parent compound porphycene and a symmetric derivative. Employing a simple two-dimensional model for the double proton transfer, which incorporates sequential and concerted motions, quantum dynamics simulations of the laser-driven dynamics are performed which demonstrate tautomerization control. Based on the orientation of the transition dipole moments, this tautomerization may lead to an estimated change in the Förster transfer coupling of about 60%.

Keywords Quantum dynamics · Proton transfer · Laser control · Molecular wires

M. K. Abdel-Latif · O. Kühn (✉)
Institut für Physik, Universität Rostock,
18051 Rostock, Germany
e-mail: oliver.kuehn@uni-rostock.de

M. K. Abdel-Latif
Chemistry Department, Faculty of Science,
Beni-Suef University, Beni-Suef, Egypt

1 Introduction

Molecular photonic wires are of considerable interest as biomimetic models for photosynthetic light-harvesting systems and as molecular devices [1]. Lindsey et al. have been the first to demonstrate directed energy transfer through a porphyrin-based wire after selective excitation of a boron-dipyrrin donor [2]. Subsequently, they described a number of different systems on the basis of multiporphyrin arrays [3–5] including, for instance, shape persistent cyclic architectures [6] or optoelectronic gates [7, 8] (for a review, see also Ref. [9]). The energy transfer in these structures is dominated by a through-bond mechanism with some dependence on the nature of the bridge linking the chromophores [10]. A different design strategy has been followed by Sauer and coworkers who have used the backbone of double-stranded DNA as a scaffold for positioning highly fluorescent chromophores [11–14] (see also Ref. [15]). Here, Förster type dipole–dipole interaction-driven transfer is the responsible mechanism for energy transfer with efficiencies close to 100% over a range of ∼14 nm.

The utilization of molecular wires in optoelectronic devices requires to have at hand a means for switching the energy transfer dynamics. Various methods such as optical excitation using UV radiation [16], electrochemical oxidation [8, 17, 18], or changing the pH value of the medium [19] have been suggested (for an overview, see also Refs. [1, 20]). This includes even the realization of photochemical logic gates as reported in Ref. [21]. Recently, we have proposed another route to switch excitation energy transfer which could operate in the ultrafast regime of a few picoseconds [22]. The idea builds on the observation that the direction of the electronic transition dipole moment, which is responsible for the coupling between chromophores in the Förster mechanism [23], depends on the positions of the two

H atoms in the porphyrin-like building blocks of molecular wires. Thus, switching between the ground state tautomers, i.e., triggering the double proton transfer (DPT) by means of an appropriately designed laser field in the infrared (IR) domain enables one to modify the strength of the Förster transfer coupling.

The aim of the present contribution is to extend the model study of Ref. [22] toward a specific molecular system and to show exemplarily to what extent laser-triggered DPT can influence the Förster transfer coupling. Specifically, we will focus on porphycene-like structures, which have rather strong hydrogen bonds (HBs) whose properties are widely adjustable by the structural design [24]. For the laser-driven DPT, the shape of the potential energy landscape is rather important. Besides energy barriers which need to be sur- mounted by excitation with a few IR photons, reactants and products should be energetically different to prevent an efficient backreaction via tunneling. Asymmetrically substituted porphycenes seem to meet these requirements. In the following, we will consider 9-actetoxy-2,7,12,17- tetra-n-propylporphycene (**3**) whose spectroscopy had been studied by Waluk and coworkers [25]. Thus, besides the specific goal of demonstrating a laser-driven switch for molecular photonic wires, our quantum chemical studies of the ground state properties and the $S_0 \rightarrow S_1$ excitation spectrum will shed some light on the effect of symmetric (**2**) and asymmetric (**3**) substitution of the porphycene parent compound (**1**) and hence will provide the theoretical basis for the assignment of the absorption spectrum.

The paper is organized as follows: Sect. 2 gives a brief summary of the quantum chemical and quantum dynamical methods. The results Sect. 3 starts with the discussion of the geometries and energetics of the stationary points of porphycene and its derivatives (see Fig. 1). Based on this information a two-dimensional (2D) model Hamiltonian is constructed in Sect. 3.2 that comprises coordinates of concerted and sequential DPT. Subsequently, the $S_0 \rightarrow S_1$ excitation spectrum is discussed in terms of the involved molecular orbitals and transition dipole moments. The laser-driven DPT dynamics will be presented in Sect. 3.5, and the final Sect. 4 concludes with a summary.

2 Methods

Geometry optimization for the electronic ground state has been performed using density functional theory (DFT) employing the B3LYP hybrid functional together with a 6- 31+G(d,p) basis set. Stationary points have been validated by means of frequency calculations. Excitation energies are obtained from time-dependent DFT (TDDFT) calculations at the optimized ground state geometries (vertical excita- tion) and using the same functional and basis set. All
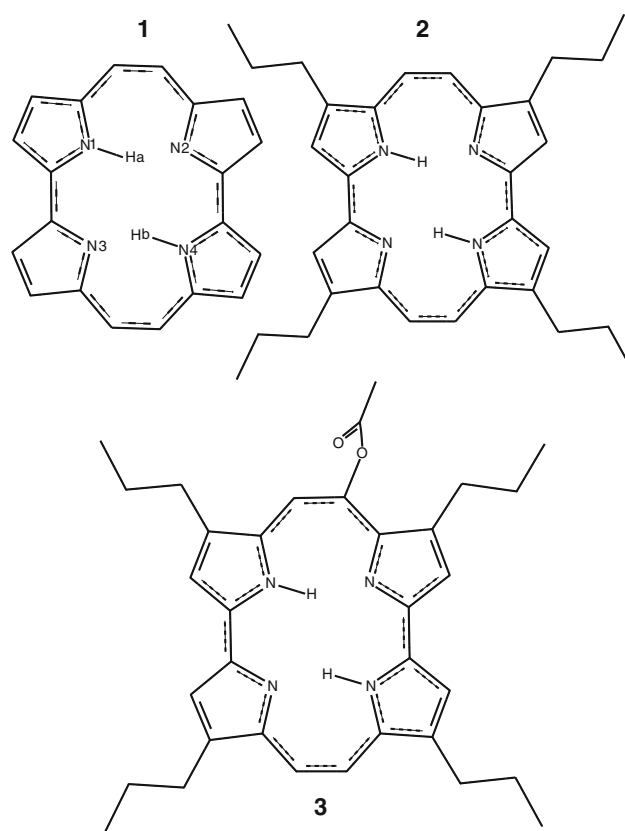

Fig. 1 Reference structures of considered porphycenes: **1** free-base porphycene, **2** tetra-n-propylporphycene, and **3** more stable trans form (Tr1) of tetra-n-propyleacetoxyporphycene

quantum chemical calculations are performed with the Gaussian 03 suite of programs [26].

The two-dimensional time-dependent Schrödinger equation has been solved using the multiconfiguration time- dependent Hartree (MCTDH) approach [27, 28] as imple- mented in the Heidelberg program package [29]. The grid was chosen according to the harmonic oscillator discrete variable representation (64 points within $[-2.5 : 2.5]a_0$). The actual propagation is performed using the variable mean field scheme in combination with a 6th order Adams- Bashforth-Moulton integrator. Using 20 single-particle functions per degree of freedom, the largest natural orbital populations have been typically on the order of 10^{-6}. Selected eigenstates of the time-independent Hamiltonian, φ_i, are obtained by improved relaxation [30].

3 Results

3.1 Optimized geometries

Ground state optimized structures of **2** show that this mol- ecule like **1** is planar in accord with Ref. [24]. Asymmetric substitution, however, causes **3** to become nonplanar with

respect to the acetoxy group. Overall, **3** has two global trans minima, Tr1 and Tr2, two local cis minima, Cis1 and Cis2, four local maxima which correspond to first-order saddle points, Ts11 to Ts22, and one global maximum being a second-order saddle point, SP2. All these structures are shown in Fig. 2, and the energetics is compiled in Table 1. In terms of the double proton transfer, SP2 is passed in the concerted mechanism, while pathways like Tr1-Ts11-Cis1-Ts21-Tr2 are followed during sequential transfer. Finally, we note from the dipole moments given in Table 1 that **3** is considerably more polar than **2**.

The energetic difference between trans and cis, which is 804 cm^{-1} for **1**, is largely unaffected by the symmetric substitution in **2**. The same holds true for the second-order transition state SP2, i.e., the barrier height for concerted DPT is about 2,260 cm^{-1}. The barrier for stepwise proton transfer which is 1,637 cm^{-1} for **1** decreases slightly to 1,514 cm^{-1} in **2**. Upon asymmetric substitution with an acetoxy group in the 9 position in **3** most notably in

comparison with **2** is the asymmetry of the two trans tautomers which amounts to 38 cm^{-1}. This rather small value is in good accord with the experimental finding of indistinguishable tautomers [25]. Further, the SP2 transition state is lowered by about 4% and the first-order saddle points and cis minima are changed in a way such as to make a stepwise DPT via Cis1 energetically more preferable.

The results on the HB geometries of **3** are compiled in Table 2 which also contains values for the trans tautomers of **1** and **2**. Comparing the most stable trans forms of the three molecules, the differences in HB parameters are rather small. Most notably again is the asymmetry, i.e., in Tr1, the HB next to the acetoxy substitution site (N_1–H_a–N_2) is slightly shorter and substantially more nonlinear when compared with N_3–H_b–N_4. The geometric signature of the energetically more preferable path for stepwise DPT can be found in the stronger contraction of N_3–H_b–N_4 in Ts11 when compared with N_1–H_a–N_2 in Ts12. The
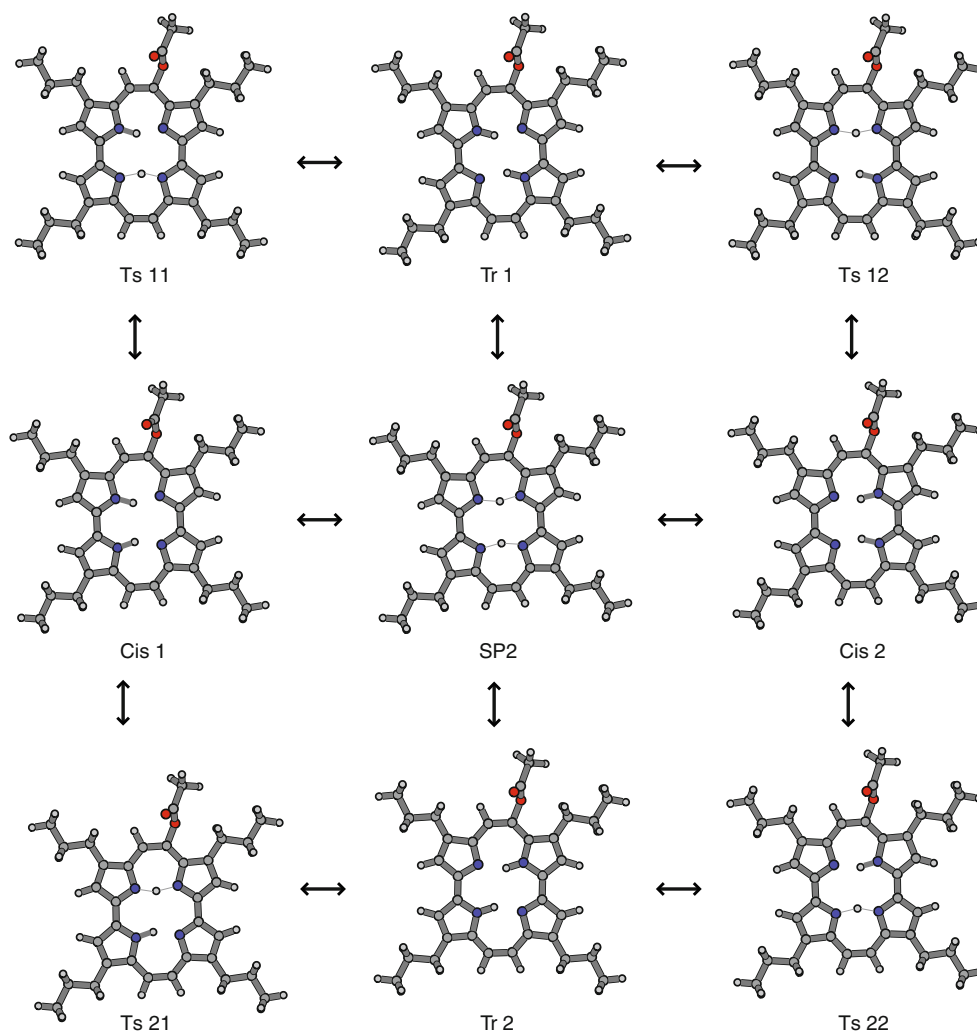

Fig. 2 Optimized geometries (B3LYP/6-31+G(d,p)) of all stationary points of **3** which are relevant for DPT

Table 1 Energies and absolute value of dipole moments of stationary points for the tautomerism of the molecules shown in Fig. 1 at the B3LYP/6-31+G(d,p) level of theory (values for **1** from Ref. [31])

Molecule	Structure	ΔE (cm^{-1})	Dipole (Debye)
3	Tr1	0	1.633
	Tr2	38	1.481
	Cis1	726	2.042
	Cis2	838	2.218
	SP2	2,169	1.635
	Ts11	1,329	1.539
	Ts12	1,505	1.865
	Ts21	1,479	1.690
	Ts22	1,461	1.834
2	Tr	0	0.002
	Cis	817	1.452
	SP2	2,263	0.000
	SP1	1,514	0.770
1	Tr	0	
	Cis	804	
	SP2	2,256	
	SP1	1,637	

transition states for the second transfer step, Ts21 and Ts22, on the other hand, have almost the same HB parameters.

3.2 Ground state model Hamiltonian

The potential energy surface for DPT in the electronic ground state will be modeled using a simple Hamiltonian which was introduced by Smedarchina and coworkers [33, 34] and which has been supplemented by asymmetric terms to mimic systems like **3** in Ref. [22]. Assuming that only the proton coordinates are active on a surface where all

other coordinates are adiabatically adjusted, we have the following Hamiltonian ($m = 2m_H$)

$$H = -\frac{\hbar^2}{2m}\left(\frac{\partial^2}{\partial x_s^2} + \frac{\partial^2}{\partial x_a^2}\right) + U_{\text{sym}}(x_s, x_a) + U_{\text{asym}}(x_s, x_a). \tag{1}$$

Here, symmetric and asymmetric transfer coordinates x_s and x_a, respectively, have been introduced. They are defined with respect the to linear displacements of the two H atoms along the hydrogen bonds, x_1 and x_2, as follows: $x_s = (x_1 + x_2)/2$ and $x_a = (x_1 - x_2)/2$. The symmetric potential, $U_{\text{sym}}(x_s, x_a)$, originates from two bilinearly coupled quartic oscillators when expressed in the coordinates of the individual H atoms x_1 and x_2. After introduction of the transfer coordinates x_s and x_a, this gives:

$$U_{\text{sym}}(x_s, x_a) = 2U_0 + \frac{U_0}{x_0^2}\left[(g-4)x_a^2 - (g+4)x_s^2\right] + \frac{2U_0}{x_0^4}(x_s^4 + x_a^4 + 6x_s^2 x_a^2). \tag{2}$$

Here, g is the coupling constant, $\pm x_0$ are the minima for the uncoupled double minimum potential which has a barrier height of U_0. Asymmetry can be introduced by the following term:

$$U_{\text{asym}}(x_s, x_a) = \frac{\alpha_{\text{trans}} U_0}{x_0} x_s + \frac{\alpha_{\text{cis}} U_0}{x_0} x_a \tag{3}$$

where α_{trans} and α_{cis} are dimensionless parameters characterizing the detuning between the trans and cis states, respectively.

The parameters for this Hamiltonian have been obtained by fitting to the quantum chemical results of Table 1. The resulting potential energy surface is plotted in Fig. 3, and the fitting parameters are given in the figure caption. Note that while the minima and the SP2 maximum are in good

Table 2 Geometries of the HBs in **3** (and for Tr in **1** and **2**) at the B3LYP/6-31+G(d,p) stationary points (bond lengths in Ångstrom, angles in degrees, data for **1** are taken from Ref. [32])

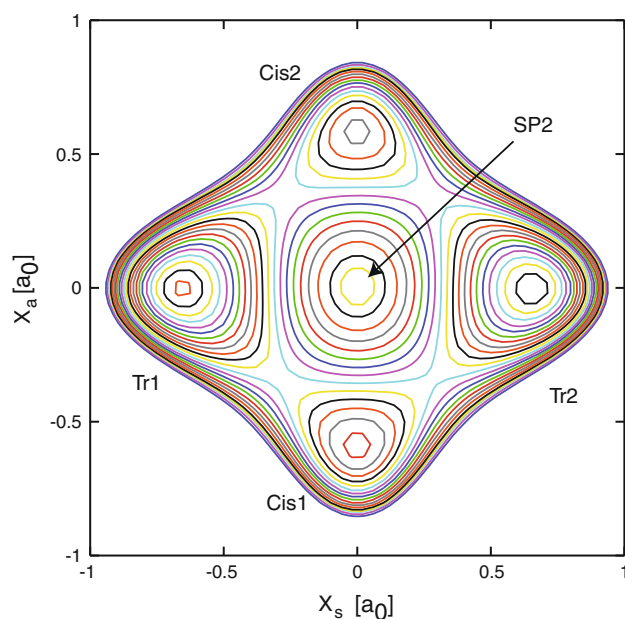| Structure	N_1–H_a	N_2–H_a	N_1–N_1	$\angle N_1$–H_a–N_2	N_3–H_b	N_4–H_b	N_3–N_4	$\angle N_3$–H_b–N_4
Tr1	1.05	1.68	2.65	152.9	1.05	1.70	2.67	150.9
Tr2	1.68	1.05	2.65	153.0	1.67	1.05	2.66	154.9
Cis1	1.61	1.07	2.61	155.1	1.06	1.64	2.62	152.6
Cis2	1.07	1.61	2.61	154.0	1.60	1.07	2.62	156.5
SP2	1.30	1.26	2.51	159.4	1.28	1.27	2.50	159.1
Ts11	1.06	1.61	2.60	153.1	1.26	1.30	2.52	159.2
Ts12	1.30	1.26	2.52	159.6	1.57	1.07	2.58	154.8
Ts21	1.26	1.31	2.52	159.2	1.07	1.57	2.58	155.3
Ts22	1.57	1.07	2.59	156.8	1.31	1.25	2.52	158.9
2	1.05	1.69	2.67	152.6				
1	1.05	1.68	2.66	152.8				

Fig. 3 Two-dimensional model potential according to Eq. 1 for the DPT in **3**. The parameters are $U_0 = 876\,\mathrm{cm}^{-1}$, $x_0 = 0.624a_0$, $g = 0.435$, $\alpha_{trans} = 0.0095$, and $\alpha_{cis} = 0.034$. The barrier height for concerted transfer is $2{,}169\,\mathrm{cm}^{-1}$. The energetic difference between the two trans minima is $38\,\mathrm{cm}^{-1}$, and the energies of the cis minima are 725 and $838\,\mathrm{cm}^{-1}$ (contour lines are in steps of $400\,\mathrm{cm}^{-1}$ from 400 to $8{,}800\,\mathrm{cm}^{-1}$)

agreement with the quantum chemistry results, the simple form of the potential does not provide enough flexibility for obtaining all first-order transition states at the same time with comparable accuracy. The deviations range from 51 to $169\,\mathrm{cm}^{-1}$, which are, however, still acceptable given the overall approximate nature of the treatment.

For the interaction with the laser field, we assume that the permanent dipole moment depends only linearly on the coordinates, i.e.,

$$H_{\mathrm{field}}(t) = -(d_a x_a + d_s x_s)E(t) \qquad (4)$$

where $d_{a/s}$ is the derivative of the dipole moment with respect to $x_{a/s}$. The permanent dipole moment changes mostly along one polarization direction (x, cf. Fig. 5). Assuming the laser being linearly polarized along that direction and making a linear interpolation between the minimum configurations, we obtain $d_s = -0.028e$ and $d_a = 0.150e$.

For the laser field, we will use the following form

$$E(t) = \sum_{i=1,2} E_{0,i} \cos(\omega_i t) \exp(-(t - t_{0,i})^2 / 2\tau_i^2) \qquad (5)$$

that facilitates the consideration of the so-called pump-dump control mechanism [35, 36]. In Eq. 5 $E_{0,i}$ is the amplitude, ω_i the carrier frequency, and τ_i the temporal width of the pulse centered at $t_{0,i}$.

3.3 Molecular orbitals and excited states

In the following, we will discuss the $S_0 \rightarrow S_1$ transition, which contributes to the Q absorption band. Results of TDDFT calculations are compared with experimental data in Table 3 for the different compounds. First, we notice that TDDFT gives excitation energies that exceed the experimental ones by about $1{,}500$–$2{,}100\,\mathrm{cm}^{-1}$. Most of this difference must be attributed to the method itself (see, e.g., systematic study in Ref. [38]). Further deviations might be due to the fact that the experimental values correspond to the 0–0 transitions whereas the calculations are performed for a vertical excitation. Comparing the experimental spectra of porphycenes in gas and condensed phases, the environmental effects (e.g., a nitrogen matrix in Ref. [25]) are negligible [24].

Let us focus on the tautomerization of **3**. As discussed in Sect. 3.1, the energetic asymmetry in the electronic ground state is rather small. The measured splitting in the $S_0 \rightarrow S_1$ transition, however, gave evidence for a considerable asymmetry in the excited states of $285\,\mathrm{cm}^{-1}$ [25]. The assignment of the most stable tautomer in the S_1 excited state has been based on a semiempirical ZINDO/S calculation. Considering Table 3, we notice that the agreement of the splitting in the $S_0 \rightarrow S_1$ transitions ($278\,\mathrm{cm}^{-1}$) is rather good, thus giving strong support for the experimental conclusions in Ref. [25].

The $S_0 \rightarrow S_1$ transitions are of $\pi \rightarrow \pi^*$ type with participation of the π (HOMO, HOMO-1) and π^* (LUMO, LUMO+1) molecular orbitals (MOs). These orbitals are shown for the different molecules in Fig. 4, and orbital coefficients are compiled in Table 3. The main contributions to the $S_0 \rightarrow S_1$ transition in **1** and **2** are of HOMO-1 $\rightarrow$ LUMO type (see also Ref. [39]). The same holds true for the less stable tautomer Tr2 of **3**. Interestingly, in tautomer Tr1 of **3**, this transition is of HOMO $\rightarrow$ LUMO type.

Table 3 Excitation energies (in cm^{-1}) and oscillator strengths (in parenthesis) obtained at the TD-DFT B3LYP/6-31+G(d,p) level of theory

Struct.	Calc.	Exp.	Leading excitation
3(Tr1)	17,392 (0.15)	15,708	144 → 145 (0.58)
3(Tr2)	17,670 (0.13)	15,993	143 → 145 (0.58)
2	17,536 (0.14)	15,983	128 → 130 (0.48)
1	17,904 (0.12)	16,000	80 → 82 (0.56)

The calculated values for the different structures are compared with the experimental assignment from Refs. [25] (**2**, **3**) and [37] (**1**). Note that the experimental values correspond to the respective 0–0 transition

Fig. 4 Molecular orbitals relevant for the $S_0 \rightarrow S_1$ transition (cf. Table 3) for molecules **1**, **2**, and the two tautomers of **3**. The orbital numbers are 80–83 (**1**), 128–131 (**2**), and 143–146 (**3**)
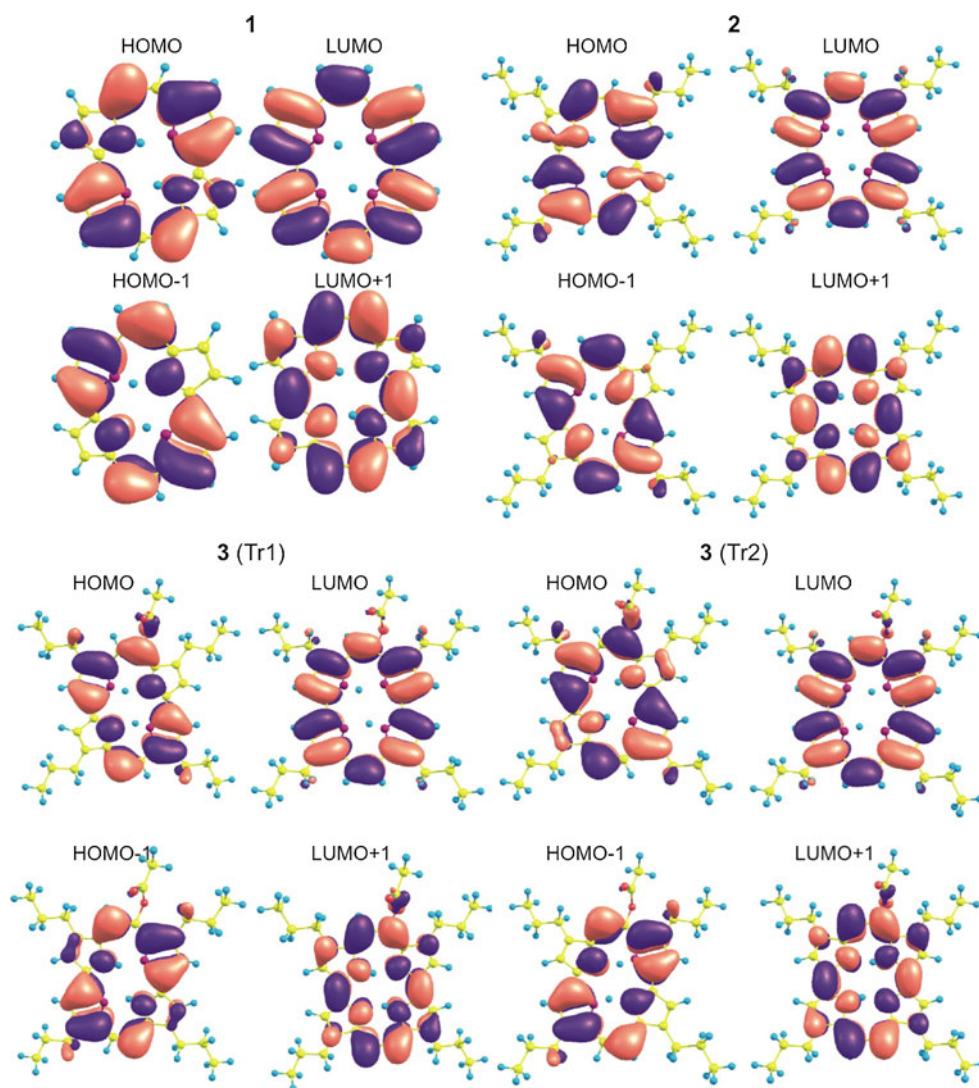
Comparison of the MOs of Tr1 and Tr2 shows that the order of HOMO and HOMO-1 is *reversed* upon tautomerization.

A closer look at the orbitals reveals the effect of symmetric and asymmetric substitutions. Going from **1** to **2**, some electron density appears at those alkyl chains that are opposite to the position of the hydrogen-bonded H atom. Overall, however, the MOs are rather similar, i.e., in the HOMO, there is a *p*-orbital at those nitrogens, which are bonded to the central hydrogens whereas there is no electron density at the "free" nitrogen atoms. In the HOMO-1, this situation is reversed. Asymmetric substitution causes a disturbance of the porphycene π-system by the acetoxy group with the effect being different for the two tautomers. Tr2 of **3** resembles the HOMO in **1** and **2** with some electron density at the acetoxy group. In Tr1 of **3**, the presence of the latter electron density renders the Tr2-HOMO-1 to become more stable than the Tr2-HOMO.

3.4 Transition dipole orientation

The directions of the transition dipole moments for the $S_0 \rightarrow S_1$ transitions of the different molecules are compiled in Fig. 5. Comparing **1** and **2**, we notice that symmetric substitution has almost no effect on the direction of the transition dipole moments. Furthermore, both cases show the well-known 90° change in the transition dipole moment upon tautomerization. The presence of the acetoxy group in **3**, however, changes this picture due to the polarity introduced by the oxygen atoms. Most notably is the fact that the tautomerization causes a tilt of the transition dipole moment by about 50° only.

Let us assume that **3** is built into a molecular photonic wire. The Förster energy transfer coupling between different molecular subunits of the wire called donor (D) and acceptor (A) is given by [23]
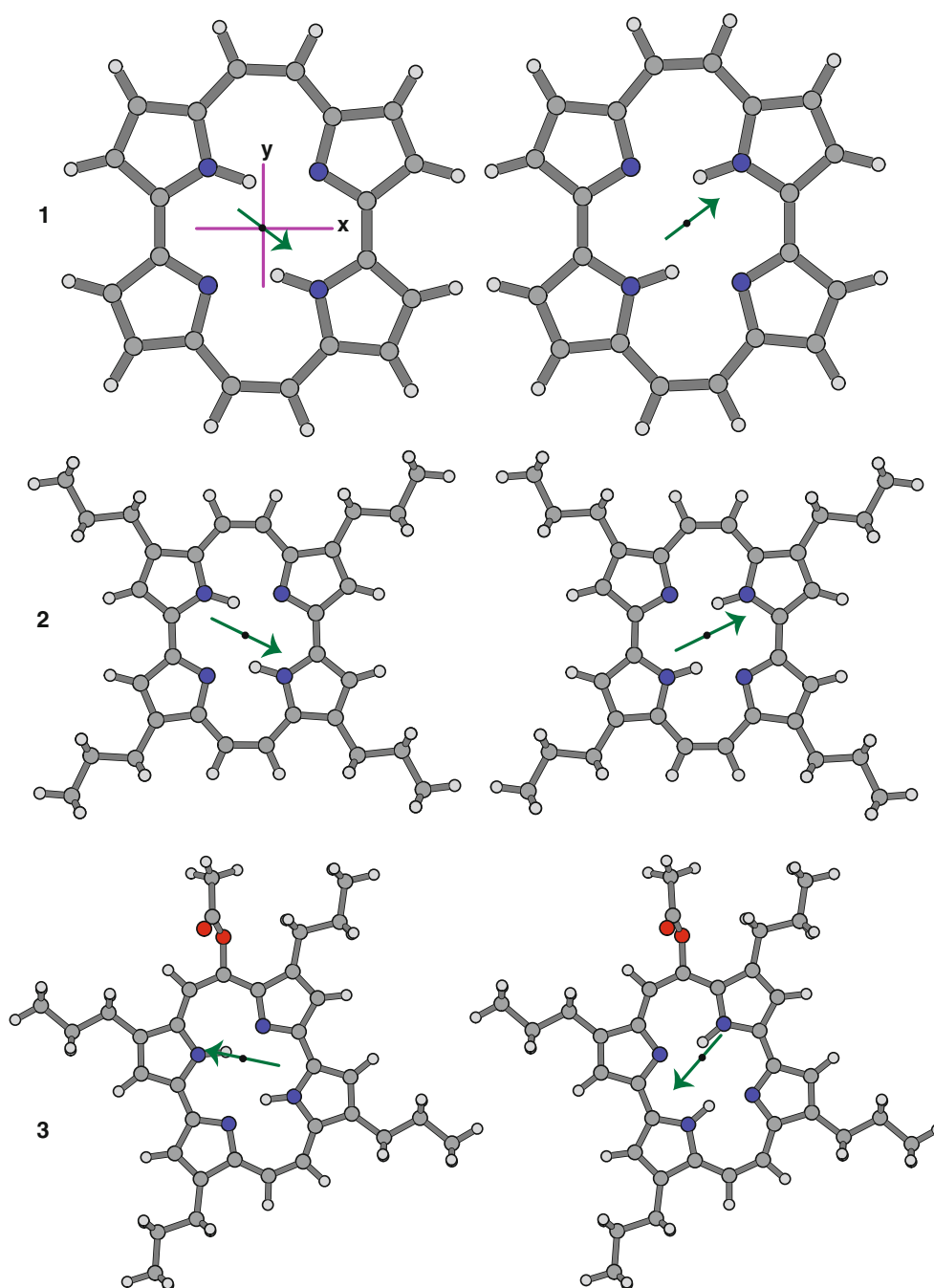
Fig. 5 Transition dipole moment vectors for structures **1** (*left*) (1.252, −0.950), **2** (*left*) (−1.489, 0.672), **3**(Tr1) (−1.652, 0.356), and **3**(Tr2) (−1.042, 1.174) (in Debye)

$$J_{DA} = \kappa_{DA} d_{10}^{(D)} d_{10}^{(A)} \frac{1}{R_{DA}^3}. \tag{6}$$

Here, $d_{10}^{(A/D)}$ is the magnitude of the transition dipole moment for the $S_0 \to S_1$ transition and R_{DA} is the distance between donor and acceptor. Most important for the present discussion is the orientational factor given by

$$\kappa_{DA} = \mathbf{n}_A \cdot \mathbf{n}_B - 3(\mathbf{e}_{DA} \cdot \mathbf{n}_D)(\mathbf{e}_{DA} \cdot \mathbf{n}_A), \tag{7}$$

where $\mathbf{n}_{D/A}$ and $\mathbf{e}_{DA}$ are the unit vectors pointing in the directions of the transition dipole moment of D/A and the center-to-center DA distance, respectively.

In order to estimate the effect of DPT on the Förster transfer coupling and in particular on the orientational factor, we suppose that **3** is built into the wire such that the neighboring unit has a transition dipole moment like structure **1**. This could be the case, for instance, for the

widely used porphyrins. Let us further assume that $\mathbf{e}_{DA}$ points along the x-direction. In this case, we obtain $\kappa_{DA}(Tr1) = 1.43$ and $\kappa_{DA}(Tr2) = 0.60$. In other words, the transfer coupling changes by about 60% as a consequence of the tautomerization.

3.5 Laser control of DPT in the electronic ground state

In the following, we will investigate the possibility to control the DPT in **3** using a simple two-pulse pump-dump scheme involving an intermediate state that is energetically above the reaction barrier for concerted DPT (cf. Fig. 6). The initial state is localized mostly in the Tr1 well, while the final state lies mostly in the Tr2 well. Due to the low barrier and the small asymmetry, both states have finite probabilities in the respective other wells. The goal is to find an electric field of the form given by Eq. 5, for which the first (pump) pulse populates the intermediate state and the second (dump) pulse triggers a transition from this intermediate to the reactant state. This scheme operates in complete analogy to other isomerization reactions studied previously, such as the single H-atom transfer in malonaldehyde [36] or the cope rearrangement in semibullvalenes [35]. The parameters for the present case of DPT were chosen as follows: First, the field strength is fixed at a certain value and the pulse length is increased starting from 800 fs until the intermediate state population reaches a maximum. For this pulse length, the field amplitude is changed around its starting value to check whether the intermediate state population can be increased. The carrier frequency is chosen to correspond to the respective transition frequency. The same procedure is followed independently for the dump pulse by letting it start immediately
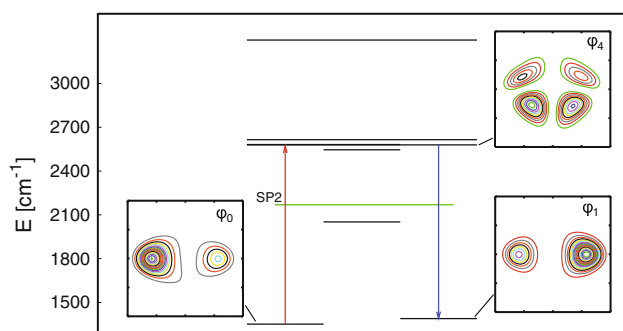

Fig. 7 *Upper panel* electric field for the pump-dump control scheme (pulse parameters: $E_{0,1} = 7$ mE$_h$/ea$_0$), $\omega_1 = 1,111$ cm^{-1}, $t_{0,1} = 2,200$ fs, and $\tau_1 = 650$ fs; $E_{0,2} = 4$ mE$_h$/ea$_0$), $\omega_2 = 1,055$ cm^{-1}, $t_{0,2} = 3,750$ fs, and $\tau_2 = 200$ fs). Lower panel: Population dynamics of the states φ_0, φ_1, and φ_4

after the pump pulse. This gave a total pulse duration of 5 ps during which the population of the intermediate state showed a plateau, which allowed us to shift the dump pulse such that pump and dump pulse partly overlap (cf. Fig. 7).

The progress of the laser-driven reaction can be followed by calculating the populations of vibrational eigenstates of the model Hamiltonian. A representation of the energy level scheme is given in Fig. 6 that also shows the probability density of those states that dominate the dynamics. The chosen above-barrier transition state involves an excitation of the asymmetric stretching coordinate x_a which triggers the reaction to occur mostly along the stepwise pathway (see also Ref. [22]). Furthermore, it is seen that the probability density has a higher weight in that part of the potential where $x_a < 0$, implying that there is a preference for the Cis1 minimum to be visited during the dynamics. According to our previous study [22], this is due to the higher stability of Cis1 when compared with Cis2. Finally, we note that there are several states in the region of the chosen intermediate state φ_4, thus, state selective population will be more easily achieved using long pulses when compared, e.g., with the NH-vibrational stretching frequency.

Fig. 6 Energy level scheme of the model Hamiltonian for **3** including the probability densities of those states that dominate the dynamics. The lengths of the *horizontal lines* indicate the area of delocalization of the wave function along the x_s coordinate. The *green line* corresponds to the energy of the SP2 barrier. The vibrational eigenstates have been obtained using the improved relaxation scheme within MCTDH [30]. The pathway of laser-driven pump-dump control is marked by *vertical arrows*. The density plots cover the range $[-1:1]a_0$ along the *vertical* x_a and the *horizontal* x_s axes
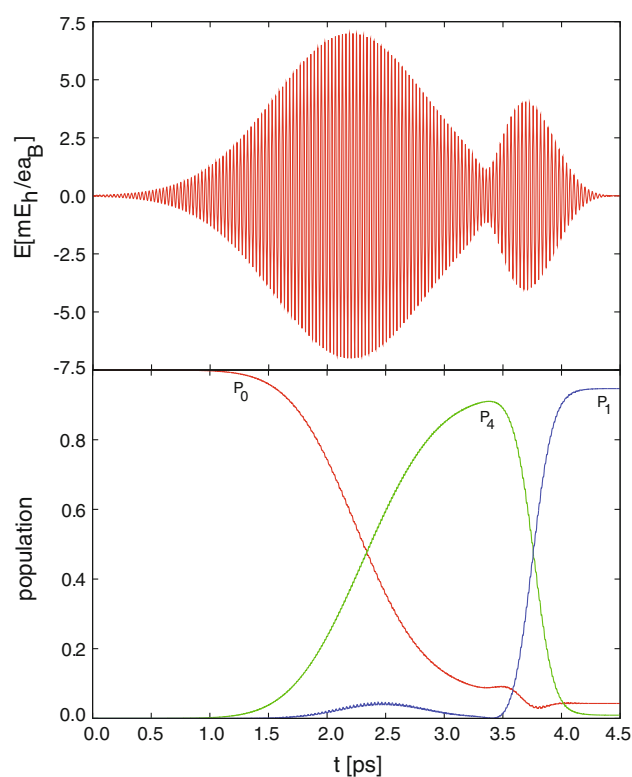
The optimized field and selected state populations are shown in Fig. 7. The pump pulse excites the system from the ground state, φ_0, to the intermediate state, φ_4, while the dump pulse de-excites this population to the target state φ_1. The maximum intermediate state population is 91%, reached around 3.4 ps. At this time, however, the dump pulse is already transferring population from φ_4 to the target state φ_1. The overall duration of the laser-induced DPT process is 4.5 ps, and the final population of the target state is 95%. Two minor features seen in Fig. 7 deserve a comment. Around 2.4 ps, there is some transient population of the target state already due to the pump pulse. Later on around 3.6 ps, the dump pulse also is seen to further depopulate the initial ground state. Both effects can be traced to the fact that the energetic separation between the two transitions is only 56 cm^{-1}, i.e., they can be simultaneously addressed by the laser pulse spectra.

4 Conclusions

In summary, we have investigated the possibility to use IR laser-controlled double proton transfer in the electronic ground state of asymmetrically substituted porphycene as a way of influencing the direction of the $S_0 \rightarrow S_1$ transition dipole moment. This gives a means for changing the dipole–dipole interaction between neighboring chromophores in a molecular photonic wire. The estimated effect amounts to a 60% change in the transfer coupling which could be used to design a molecular switch operating on a timescale of a few picoseconds and being, in principle, reversible.

Needless to say that this proof-of-principle study calls for several extensions. First, the two-dimensional model of double proton transfer needs to be extended to account for heavy atom motions of the scaffold, e.g., using the Cartesian reaction surface approach [40]. Indeed, Waluk and coworkers showed that the coupling to this type of motions may have a strong influence on the dynamics [41–43]. It is to be expected that intramolecular vibrational energy redistribution is effective on the timescale of a few picoseconds covered in the present study, i.e., either substantially shorter pulses have to be used or more sophisticated pulse forms need to be devised, which, e.g., make use of the promoting character of certain scaffold modes. Second, a suitable design for a molecular photonic wire containing a DPT switching unit has to be found. This implies not only a favorable orientation of the transition dipoles of neighboring units but also the dominance of through-space Förster transfer over through-bond energy transfer.

References

1. Balzani V, Credi A, Venturi M (2003) Molecular devices and machines. Wiley-VCH, Weinheim
2. Wagner RW, Lindsey JS (1994) J Am Chem Soc 116:9759
3. Wagner R, Johnson T, Lindsey J (1996) J Am Chem Soc 118:11166
4. Hsiao J, Krueger B, Wagner R, Johnson T, Delaney J, Mauzerall D, Fleming G, Lindsey J, Bocian D, Donohoe R (1996) J Am Chem Soc 118:11181
5. Seth J, Palaniappan V, Wagner R, Johnson T, Lindsey J, Bocian D (1996) J Am Chem Soc 118:11194
6. Li J, Ambroise A, Yang S, Diers J, Seth J, Wack C, Bocian D, Holten D, Lindsey J (1999) J Am Chem Soc 121:8927
7. Ambroise A, Wagner R, Rao P, Riggs J, Hascoat P, Diers J, Seth J, Lammi R, Bocian D, Holten D, Lindsey J (2001) Chem Mater 13:1023
8. Lammi R, Wagner R, Ambroise A, Diers J, Bocian D, Holten D, Lindsey J (2001) J Phys Chem B 105:5341
9. Holten D, Bocian D, Lindsey J (2002) Acc Chem Res 35:57
10. Song H, Taniguchi M, Diers JR, Kirmaier C, Bocian DF, Lindsey JS, Holten D (2009) J Phys Chem B 113:16483
11. Heilemann M, Tinnefeld P, Mosteiro G, Garcia-Parajo M, Hulst NV, Sauer M (2004) J Am Chem Soc 126:6514
12. Tinnefeld P, Heilemann M, Sauer M (2005) Chem Phys Chem 6:217
13. Sanchez-Mosteiro G, van Dijk EMHP, Hernando J, Heilemann M, Tinnefeld P, Sauer M, Koberlin F, Patting M, Wahl M, Erdmann R, van Hulst NF, Garcia-Parajo MF (2006) J Phys Chem B 110:26349
14. Heilemann M, Kasper R, Tinnefeld P, Sauer M (2006) J Am Chem Soc 128:16864
15. Vyawahare S, Eyal S, Mathews K, Quake S (2004) Nano Lett 4:1035
16. Bahr J, Kodis G, de la Garza L, Lin S, Moore A, Moore T, Gust D (2001) J Am Chem Soc 123:7124
17. Wagner R, Lindsey J, Seth J, Palaniappan V, Bocian D (1996) J Am Chem Soc 118:3996
18. Akasaka T, Otsuki J, Araki K (2002) Chem Eur J 8:130
19. Albelda M, Diaz P, Garcia-Espana E, Lima J, Lodeiro C, de Melo J, Parola A, Pina F, Soriano C (2002) Chem Phys Lett 353:63
20. Otsuki J, Akasaka T, Araki K (2008) Coord Chem Rev 252:32
21. Straight SD, Liddell PA, Terazono Y, Moore TA, Moore AL, Gust D (2007) Adv Funct Mater 17:777
22. Abdel-Latif MK, Kühn O (2010) Chem Phys 368:76
23. May V, Kühn O (2011) Charge and energy transfer dynamics in molecular systems, 3rd revised and enlarged edition. Wiley-VCH, Weinheim
24. Waluk J (2007) In: Hynes J, Klinman J, Limbach H-H, Schowen R (eds) Hydrogen transfer reactions. VCH-Wiley, Weinheim, p 245
25. Gil M, Jasny J, Vogel E, Waluk J (2000) Chem Phys Lett 323:534
26. Frisch MJ et al (2004) Gaussian 03, Revision C.02. Gaussian Inc, Wallingford
27. Meyer H-D, Manthe U, Cederbaum LS (1990) Chem Phys Lett 165:73
28. Beck MH, Jäckle A, Worth GA, Meyer H-D (2000) Phys Rep 324:1
29. Worth G, Beck M, Jäckle A, Meyer H-D (2007) The MCTDH package, Version 8.4. University of Heidelberg, Heidelberg
30. Meyer H-D, Quere FL, Leonard C, Gatti F (2006) Chem Phys 329:179
31. Smedarchina Z, Shibl MF, Kühn O, Fernández-Ramos A (2007) Chem Phys Lett 436:314

32. Shibl MF, Pietrzak M, Limbach H-H, Kühn O (2007) Chem Phys Chem 8:315
33. Smedarchina Z, Siebrand W, Fernandez-Ramos A (2007) J Chem Phys 127:174513
34. Smedarchina Z, Siebrand W, Fernández-Ramos A, Meana-Pañeda R (2008) Z Phys Chem 222:1291
35. Korolkov MV, Manz J, Paramonov GK (1996) J Chem Phys 105:10874
36. Došlić N, Kühn O, Manz J (1998) Ber Bunsenges Phys Chem 102:292
37. Waluk J, Muller M, Swiderek P, Kocher M, Vogel E, Hohlneicher G, Michl J (1991) J Am Chem Soc 113:5511
38. Parac M, Grimme S (2002) J Phys Chem A 106:6844
39. Sobolewski AL, Gil M, Dobkowski J, Waluk J (2009) J Phys Chem A 113:7714
40. Giese K, Petković M, Naundorf H, Kühn O (2006) Phys Rep 430:211
41. Waluk J (2006) Acc Chem Res 39:945
42. Waluk J (2009) Chem Phys Chem 10:761
43. Walewski L, Waluk J, Lesyng B (2010) J Phys Chem A 114:2313